

# The James Webb Space Telescope North Ecliptic Pole Time-Domain Field – I: Field Selection of a JWST Community Field for Time-Domain Studies

ROLF A. JANSEN<sup>1</sup> AND ROGIER A. WINDHORST<sup>1</sup>

<sup>1</sup>*School of Earth & Space Exploration, Arizona State University, Tempe, AZ 85287-1404, USA*

(Received 2018 July 13; Accepted 2018 September 24)

## Abstract

We describe the selection of the *James Webb Space Telescope* (JWST) North Ecliptic Pole (NEP) Time-Domain Field (TDF), a  $\gtrsim 14'$  diameter field located within JWST's northern Continuous Viewing Zone (CVZ) and centered at (RA, Dec)<sub>J2000</sub> = (17:22:47.896, +65:49:21.54). We demonstrate that this is the *only* region in the sky where JWST can observe a clean (i.e., free of bright foreground stars and with low Galactic foreground extinction) extragalactic deep survey field of this size *at arbitrary cadence* or at *arbitrary orientation*, and without a penalty in terms of a raised Zodiacal background. This will crucially enable a wide range of new and exciting time-domain science, including high redshift transient searches and monitoring (e.g., SNe), variability studies from Active Galactic Nuclei (AGN) to brown dwarf atmospheres, as well as proper motions of possibly extreme scattered Kuiper Belt and Inner Oort Cloud Objects, and of nearby Galactic brown dwarfs, low-mass stars, and ultracool white dwarfs. A JWST/NIRCam+NIRISS GTO program will provide an initial 0.8–5.0 $\mu$ m spectrophotometric characterization to  $m_{AB} \sim 28.8 \pm 0.3$  mag of four orthogonal “spokes” within this field. The multi-wavelength (radio through X-ray) context of the field is in hand (ground-based near-UV–visible–near-IR), in progress (VLA 3 GHz, VLBA 5 GHz, HST UV–visible, Chandra X-ray, IRAM 30m 1.3 and 2 mm), or scheduled (JCMT 850 $\mu$ m). We welcome and encourage ground- and space-based follow-up of the initial GTO observations and ancillary data, to realize its potential as an ideal JWST time-domain *community field*.

*Keywords:* dark ages, reionization, first stars — galaxies: active — galaxies: evolution — galaxies: high-redshift — supernovae: general — surveys — time-domain science

## 1. INTRODUCTION

In an age when surveys with the Panoramic Survey Telescope and Rapid Response System (Pan-STARRS; Kaiser et al. 2002), Large Synoptic Survey Telescope (LSST; Tyson 2002), *Euclid* (Laureijs et al. 2010), and Wide Field Infrared Survey Telescope (*WFIRST*; Gehrels et al. 2015) are or will soon allow time domain studies of relatively faint objects within our Solar System, Galactic neighborhood and beyond, as well as at cosmological distances and associated large look-back times, one may ask to what extent the *James Webb Space Telescope* (JWST; Gardner et al. 2006; Kalirai 2018) can serve as a time-domain survey facility. Whereas LSST's limit for variability studies over a large portion of the sky in the near-UV–near-IR reaches to  $m_{AB} \lesssim 24$  mag ( $10\sigma$ ) per  $2 \times 15$  s visit on time-scales of  $\sim 15$  min–1 hour (Tyson 2002; Ivezić 2014; LSST Science Collaboration et al. 2017), JWST/NIRCam (e.g., Horner & Rieke 2004; Greene et al. 2012) could potentially reach  $m_{AB} \sim 26.8$ –28.3 mag ( $10\sigma$ ) per epoch in the near–mid-IR on similar time-scales in a suit-

ably dark survey field<sup>1</sup>. This would enable a wide range of new and exciting time-domain science in an unexplored magnitude regime, including high redshift transient searches and monitoring (e.g., Type Ia SNe to  $z \sim 5$  and Core Collapse SNe to  $z \sim 1.5$  (Graur et al. 2014; Rodney et al. 2014, 2015b; Strolger et al. 2015; Mesinger et al. 2006) and Pair Instability SNe in the Epoch of Reionization (Pan, Kasen, & Loeb 2012; Gal-Yam 2012; Nicholl et al. 2013; Whalen et al. 2013, 2014); variability studies from (weak) Active Galactic Nuclei (AGN; e.g., MacLeod et al. 2011) to brown dwarf atmospheres (Artigau et al. 2009; Buenzli et al. 2014; Radigan et al. 2014; Rajan et al. 2015); as well as perhaps proper motions of extreme scattered Kuiper Belt, inner Oort Cloud Objects and comets on their way in toward the inner Solar System, and of nearby Galactic brown dwarfs and low-mass stars (Ryan et al. 2011; Ryan & Reid 2016), and ultracool white dwarfs (Harris et al. 2006; Catalán et al. 2013).

Shortly after insertion of the JWST in an Earth-Sun L2 halo orbit in 2021, it will start its program of Early Release Science (ERS) observations, Guaranteed Time Observations

Corresponding author: Rolf A. Jansen  
Rolf.Jansen@asu.edu

<sup>1</sup> As reported by the JWST ETC (Pontoppidan et al. 2016) v1.2 available at <https://jwst.etc.stsci.edu/>.

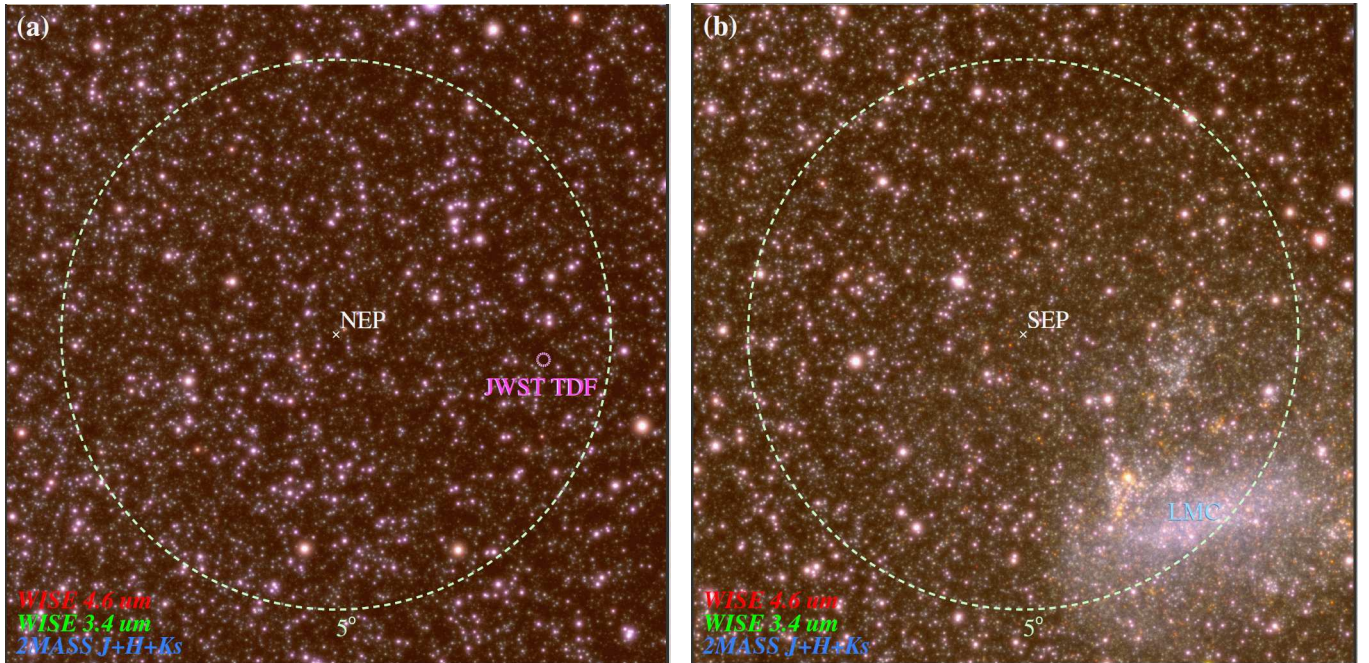


**Figure 1.** Near-infrared color composites of *JWST*’s [a] northern, and [b] southern continuous viewing zone (CVZ; indicated by the pale green dashed circle with a radius of  $5^\circ$ ). In each  $12^\circ \times 12^\circ$  image, 2MASS  $J+H+K_s$ , *WISE*  $3.4\mu\text{m}$ , and *WISE*  $4.6\mu\text{m}$  images are shown in blue, green, and red hues. For display purposes only, to better perceive source over-densities and relative brightnesses over such a wide area of sky, the constituent images were smoothed to an effective core resolution of  $\sim 1.3'$ , with a halo of  $\sim 5.7'$  (FWHM). The stretch of the images contributing to each of the two color composites is identical. *JWST*’s southern CVZ is dominated by the Large Magellanic Cloud (LMC) and a denser distribution of Galactic stars, rendering it less suitable for deep extragalactic surveys with *JWST*/NIRCam, while the northern CVZ has portions that appear relatively empty of sources that are bright at these wavelengths. The very best region selected in the northern CVZ (see §3) is indicated by a small, dotted, magenta circle with a radius of  $7'$  and labeled “*JWST* TDF”.

(GTO) by the instrument teams and Interdisciplinary Scientists (IDS), and General Observer (GO) observations. For most locations on the sky, Sun avoidance, power generation, and shielding requirements of the cryogenic telescope combine to restrict object visibility to two time intervals per year (with a duration that depends on ecliptic latitude), except within  $\sim 5^\circ$  of the Ecliptic Poles, where *JWST* will have two continuous viewing zones (CVZs) in which targets are observable year-round. Of these two small regions in the sky, the North Ecliptic Pole (NEP) CVZ constitutes relatively more empty sky; the Large Magellanic Cloud (LMC) and (associated) large-scale Galactic structures occupy much of the area within the southern CVZ, as can be seen by comparing the near-IR color composites of Fig. 1a,b and the maps of Galactic foreground reddening of Fig. 2a,b.

The orientation of *JWST*’s instrument apertures on the sky will be dictated by the date of observation, with limited schedulability of off-nominal angles ( $\Delta\text{PA} < 15^\circ$ ) due to sunshield and solar panel constraints. This is in stark contrast to observations with the *Hubble Space Telescope* (*HST*), where observers can find viable solutions for a very wide range of instrument aperture orientations. In particular, it has become common practice to revisit targets with *HST* rotated over  $180^\circ$  to secure observations with large areas of overlap between a primary and a coordinated parallel instrument

at the two orientations (e.g., CANDELS; Grogin et al. 2011; Koekemoer et al. 2011).

Moreover, off-nominal orientations with *JWST* will also carry a penalty of an increased Zodiacal background, which is up to  $\sim 1.2$ – $1.4$  mag brighter in the ecliptic plane at  $1.25$ – $4.9\mu\text{m}$  than at the ecliptic poles (Kelsall et al. 1998) — and hence results in a penalty of reduced sensitivity per unit observing time. Here also, the *JWST* CVZs are the exception, where any desired orientation can be scheduled at some time during the year, and the Zodiacal background is always at a minimum. Residual variation in the background signal in the CVZs is mostly due to orientation-dependent straylight from the Milky Way, since its combined starlight can reflect off the rear surface of *JWST*’s sunshield and enter the science instrument apertures along unintended paths (Lightsey et al. 2014; Lightsey 2016). In general, the level of straylight may reach up to  $\sim 40\%$  of the Zodiacal background.

Given that *JWST*’s CVZs are located at intermediate Galactic latitudes ( $b^{\text{II}} \pm \sim 30^\circ$ ), a field that would be optimal for a deep extragalactic time-domain survey with *JWST* would also be suitable for deep Galactic time-domain science, sampling stellar and sub-stellar populations in the nearby thin and thick disk, and stars in the more distant halo of our Galaxy. Very faint brown dwarfs and late-type low-mass stars will be detectable with *JWST*/NIRCam through

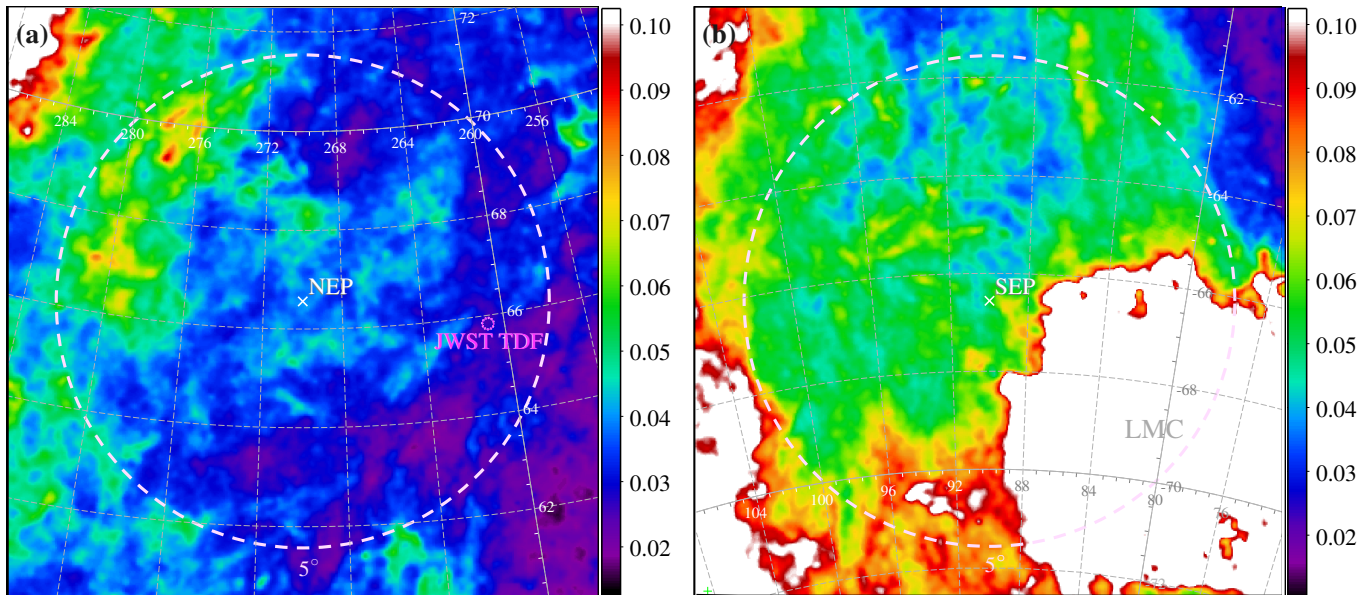


**Figure 2.** Map of  $E(B-V)$  values in the  $12^\circ \times 12^\circ$  area around (a) the North Ecliptic Pole, and (b) the South Ecliptic Pole, adopting the Schlafly & Finkbeiner (2011) recalibration of the Schlegel et al. (1998) Galactic dust reddening map. As in Fig. 1, the dashed circles with a radius of  $5^\circ$  indicate *JWST*’s Northern and Southern Continuous Viewing Zones. The location of the *JWST* Time-Domain Field (see § 3) is indicated by a magenta circle with a radius of  $7'$  in panel (a), while the LMC (labeled) and other Galactic structures occupy a large portion of the Southern CVZ in panel (b). Both panels are shown at identical stretch ( $0.01 \lesssim E(B-V) \lesssim 0.10$  mag).

both their near-infrared colors and proper motions, where the exquisite resolution of *JWST* ensures robust star–galaxy separation.

Little is known of objects in the very outer realms of our Solar System at very high ecliptic latitudes near  $\pm 90^\circ$ , should they exist. The deepest and widest high ecliptic latitude survey of trans-Neptunian objects to date ( $701 \text{ deg}^2$  to  $r_{AB} \lesssim 22.4\text{--}24.8$  mag; Petit et al. 2017) indicates that  $i \sim 90^\circ$  objects exist but are rare. Their size distribution may be flatter, but their albedo higher and color bluer, than that typical of objects in the dynamically cold population near the ecliptic plane (e.g., Schwamb et al. 2010; Shankman et al. 2016; Petit et al. 2017, and references therein). The Oort Cloud (Oort 1950) is assumed to form a roughly spherical distribution of objects that orbit the Sun at distances beyond 2000 AU out to at least  $\sim 50,000$  AU. These left-overs from the birth of our Solar System and objects captured from other star systems during close passages over the past 4.6 Gyr, if perturbed and on an inward trajectory, may be detectable with *JWST* at  $27 \lesssim m_{AB} \lesssim 29$  mag via their expected large parallaxes. A large, relatively reflective object like (90377) Sedna ( $D_\oplus = 88.1$  AU,  $d \sim 1000$  km,  $A \sim 0.32$ ,  $m_{V,\text{Vega}} \simeq 21$  mag, and  $V-K \simeq 2.1$  mag; Trujillo et al. 2005) has  $m_{K,AB} \simeq 21.7$  mag and would be directly detectable to a distance of  $\sim 500$  AU for a limiting magnitude of 29. Assuming a darker, KBO-like albedo of  $A \sim 0.04$  (e.g., Luu & Jewitt 1998), a comet nucleus as small as 10 km in diameter on its way in from the Oort Cloud would be detectable to a distance of 28–29 AU, comparable with the distance to Neptune. Outer Solar System objects within *JWST*’s CVZs would display an annual parallax, describing a circle with a

radius  $r = (180/\pi)(1/R)^\circ$ , with  $R$  their distance from the Sun in AU, and move  $\sim 148 R^{-1}''/\text{hour}$  due to their parallax (their apparent motion as a result of their orbital velocity is more than two orders of magnitude smaller). This and the low zodiacal foreground near the ecliptic poles would make the CVZs ideally suited to search for such objects, allowing detections of  $\gtrsim 10$  km comets at the distance of Neptune even within a single  $\sim 1\text{--}2$  hr visit.

In this first paper on the *JWST* North Ecliptic Pole (NEP) Time-Domain Field (TDF), we describe the selection of this new, very best target field for a deep extragalactic time-domain survey with *JWST*. For the reasons stated, we restrict our analysis to *JWST*’s CVZs, where such a survey could include the time domain from time scales of  $\sim 10$  min to 10–14 years, the anticipated maximum lifetime of *JWST* (e.g., Windhorst et al. 2018, and references therein). We further discuss considerations for a practical implementation and development of this field as both a *JWST* GTO program and as a GO community field. And we briefly list specific considerations for the ancillary ground- and space-based observations across the electromagnetic spectrum that have been secured or awarded to date, and that will each be described in detail in future papers.

## 2. SELECTION OF THE BEST FIELD FOR A DEEP EXTRAGALACTIC *JWST* SURVEY

### 2.1. Bright object concerns

The large  $\sim 6.5$  m aperture of *JWST* and the large twin  $2'2 \times 2'2$  fields of view of NIRCcam, coupled with persistence in its sensitive near- and mid-IR detectors, pose significant constraints on the presence and brightness of stars

and other objects that can be tolerated within the footprint of a deep *JWST* survey. The persistence acts as localized reductions in sensitivity and increases in image noise, and forms a record of observations that may have occurred hours earlier (and hence is a source of sample contamination). For *JWST*/NIRCam detector read-out patterns SHALLOW4, MEDIUM8, and DEEP8, appropriate for medium-deep and deep extragalactic surveys, unrecoverable saturation (i.e., when full-well charge capacity is reached already before or during the first group of reads in an integration) in a F200W observation of a flat-spectrum point source can set in for sources as faint as  $m_{AB} \simeq 18.45, 19.25,$  and  $19.80$  mag, respectively<sup>2</sup>. At mild saturation, the effects of persistence in subsequent exposures are expected to be fully modelable and correctable (Leisenring et al. 2016). This will no longer be the case for objects with  $m_{AB} \lesssim 15.5$  mag, which are bright enough to deeply saturate the NIRCam detectors. The ideal field for a deep *JWST* survey must, therefore, be devoid of any bright ( $m_{AB} < 15.5$  mag) stars that would cause such deep saturation.

## 2.2. Survey Field Size and Coordinated Parallels

If we aim to employ *HST*'s highly efficient survey strategy of revisiting a pair of primary and coordinated parallel observations with the respective instrument footprints swapped by rotating the observatory over  $180^\circ$  — possible without penalty (or at all) for *JWST* only within its two CVZs —, then we also need to take into account the projected distances between these instruments within *JWST*'s focal plane<sup>3</sup>. For NIRCam observations with parallel NIRISS observations, the corner-to-corner angular span of these cameras as projected on the sky and, hence, the absolute *minimum* diameter of a clean survey field, is  $\sim 10'.2$ . Similarly, for NIRSpec or MIRI observations with NIRCam parallels it would be  $\sim 11'.6$  or  $\sim 11'.4$ , respectively.

During experimentation with an areal survey layout that combined primary NIRCam imaging with parallel NIRISS wide-field slitless spectroscopy, we found that large dithers would be needed to span the gap between NIRCam modules A and B, and/or to advance the survey pointing by the width or height of a NIRISS footprint on the sky. This is discussed in more detail in § 4. A practical survey field size would therefore need to be significantly larger than  $\sim 10'.2$ . A field with a diameter of  $\sim 14'$  would accommodate the imaging instruments (NIRCam, NIRISS, and MIRI) in *JWST*'s focal plane, or NIRCam in combination with NIRSpec, at any orientation, and allow contiguous survey coverage with sufficient freedom for various dithering strategies. Our aim is therefore to find regions of at least this size within the *JWST* CVZs that are devoid of near-IR-bright sources.

<sup>2</sup> As reported by the *JWST* ETC (Pontoppidan et al. 2016) v1.2 available at <https://jwst.etc.stsci.edu/>.

<sup>3</sup> See *JWST Field of View*, *JWST* User Documentation [updated 2018 July 1], STScI (Baltimore, MD); <https://jwst-docs.stsci.edu/display/JTI/JWST+Field+of+View>.

## 2.3. Moving Viewport Analysis of WISE 3.4+4.6 $\mu$ m Sources

We started with an exploratory analysis of just *JWST*'s northern CVZ, by shifting a  $10' \times 10'$  viewport in steps of  $1'$  in RA and Dec through a  $\sim 5.5^\circ$  radius portion of the *WISE* Source Catalog<sup>4</sup> (Wright et al. 2010; Mainzer et al. 2011) that was centered on the NEP. We analyzed the histogram of averaged 3.4 and 4.6  $\mu$ m source magnitudes to select regions with the lowest densities of bright sources. In particular, we assigned an exponentially scaled penalty to each source within the  $10' \times 10'$  viewport, ranging from  $10^{-7}$  for sources in the 1 mag wide histogram bin centered at  $m_{AB} = 22$  mag to  $10^{10}$  for those in the bin at  $m_{AB} = 4.0$  mag (i.e., penalties increase by a factor 10 for each magnitude increase in brightness), and then summed the penalties over that viewport. *Very few*  $10' \times 10'$  regions near the NEP at a Galactic latitude of  $b^{\text{II}} \sim 30^\circ$  are devoid of stars brighter than  $m_{AB} = 16$  mag. While there are candidate regions with 3 or fewer  $m_{AB} \sim 16$  mag stars, *only one* cluster of regions stood out in that shifts of  $+2'$  or  $-2'$  are nearly as good as the very best one. That most promising target region was centered on (RA, Dec)<sub>J2000</sub> = (17:22:43, +65:49:36), and is indicated with small magenta circles to the right of and below center in Figs. 1a and 2a. The former shows that this most promising region appears indeed in a particularly dark spot in the sky. The latter, a map of Galactic reddening, shows that this lack of bright sources is not due to higher Galactic foreground extinction: the extinction here averages only  $A_V \lesssim 0.087$  mag or  $A_K \lesssim 0.015$  mag ( $E(B-V) \lesssim 0.028$  mag), where we adopt the Schlafly & Finkbeiner (2011) recalibration of the Schlegel et al. (1998) extinction map.

We then refined our moving viewport analysis, originally performed within SuperMongo<sup>5</sup>, by re-implementing it within a Fortran77 program that allowed both square and round viewports of arbitrary size, and allowed us to step through a larger area on the sky, centered on either the NEP or the SEP, with arbitrary step size. This program also assigned source penalties to individual sources directly, rather than to the sources cumulated in 1 mag wide histogram bins. We adopted a new normalization, such that a source with a mean (3.4+4.6 $\mu$ m) *WISE* source magnitude of 12.48 ( $m_{\text{Vega}}$ ; corresponding to  $m_{AB} = 15.5$  mag, given the offset of 3.02 mag between the two systems at 4  $\mu$ m<sup>6</sup>) results in a source penalty of exactly 1. Hence, the source penalties cumulated within a given viewport notionally add up to the equivalent number

<sup>4</sup> Retrieved from the NASA/IPAC Infrared Science Archive (IRSA; <http://irsa.ipac.caltech.edu/>) using a custom C-shell script, `qwisesec`, to request *WISE* and 2MASS *JHK<sub>s</sub>* photometry in  $1^\circ \times 1^\circ$  portions of the *WISE* all-sky\_4band\_p3as.psd catalog for a series of (RA, Dec) that, together, fully cover  $\sim 12^\circ \times 12^\circ$  areas around both NEP and SEP, generously encompassing the *JWST* CVZs. After retrieval, individual catalogs were concatenated and sorted, retaining the unique sources.

<sup>5</sup> <https://www.astro.princeton.edu/~rhl/sm/>

<sup>6</sup> See the Explanatory Supplement to the *WISE* All-Sky Data Release Products (R. Cutri et al.; [http://wise2.ipac.caltech.edu/docs/release/allsky/expsup/sec4\\_4h.html#conv2ab](http://wise2.ipac.caltech.edu/docs/release/allsky/expsup/sec4_4h.html#conv2ab), as updated August 7, 2017).

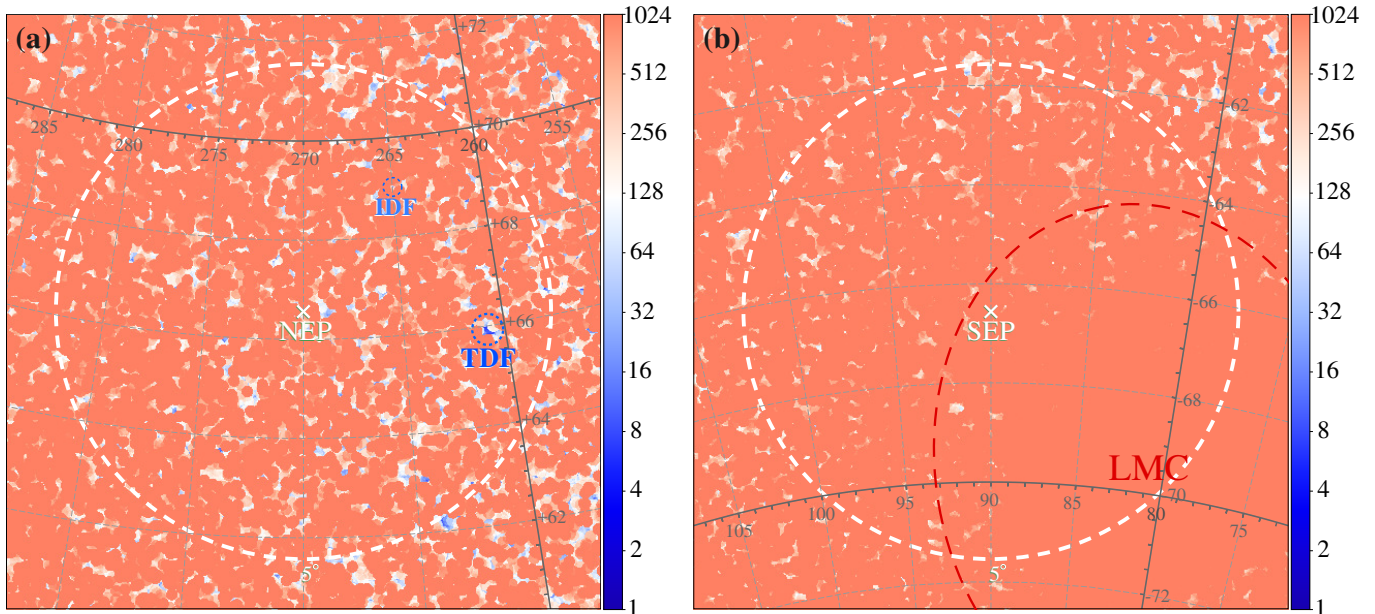


**Figure 3.** Map of  $\sim 4\mu\text{m}$  source penalties cumulated within round,  $14'$  diameter viewports stepped with  $20''$  steps through the  $12^\circ \times 12^\circ$  area around (a) the North Ecliptic Pole, and (b) the South Ecliptic Pole. As in Fig. 1, the dashed circles with a radius of  $5^\circ$  indicate *JWST*'s Northern and Southern Continuous Viewing Zones. The location of the *JWST* Time-Domain Field (TDF) and of the IRAC Dark Field (IDF; see § 3.3) are indicated with labeled, dotted circles in panel (a), while the LMC (labeled) and other Galactic structures occupy a large portion of the Southern CVZ. Penalties are normalized such that 1 corresponds to the equivalent of a single  $m_{\text{AB}} = 15.5$  mag source within a viewport. Both panels are shown at identical stretch, focusing on penalties in the 1–1024 range (the best  $14'$  diameter viewports have cumulated penalties less than 10). There are *very* few regions of this size that are devoid of sources brighter than  $m_{\text{AB}} = 15.5$  mag, appearing in dark blue hues in these maps.

of deeply saturating ( $m_{\text{AB}} = 15.5$  mag) sources within that viewport. Last, the new code was generalized to allow different weighting of  $3.4$  and  $4.6\mu\text{m}$  source magnitudes ( $3.4\mu\text{m}$  only,  $(3.4+4.6)/2 \simeq 4\mu\text{m}$ ,  $(2 \times 3.4 + 4.6)/3$ , or  $4.6\mu\text{m}$  only).

The results for round viewports with a diameter of  $14'$  (our desired *JWST* survey field size; see § 2.2) stepped through the  $12^\circ \times 12^\circ$  area centered on the NEP in  $20''$  steps is rendered in Fig. 3a and, scaled identically, for the SEP in Fig. 3b. As in our preliminary analysis, we find very few  $14'$  diameter regions that are devoid of sources brighter than  $m_{\text{AB}} = 15.5$  mag. Nonetheless, within *JWST*'s northern CVZ, a few small regions and clusters of such regions appear as dark blue shades in Fig. 3a, the very best cluster of which is still centered on  $(\text{RA}, \text{Dec})_{\text{J2000}} = (17:22:43, +65:49:36)$ . We did *not* identify any similarly clean regions within the southern CVZ.

While *JWST*'s southern CVZ will offer great opportunities for time-domain science in the LMC, we will discard it from further consideration for the purpose of any deep extragalactic field to survey the distant universe.

#### 2.4. Point Sources versus Extended Sources

Point sources at a given magnitude will have a larger impact on detector persistence than more extended sources (galaxies). For sources of the same magnitude, the brightest pixels in the latter will be several magnitudes fainter than in stellar images. We therefore verified in a 2MASS (Skrutskie et al. 2006) *JHKs* composite image with an angular resolution of  $\sim 2''$  (FWHM) that most of the  $\sim 4\mu\text{m}$ -bright *WISE*

sources (nominal FWHM  $\sim 6''1$ – $6''4$ ) within the best cluster of clean  $14'$  diameter regions are indeed Galactic stars, and proved that the best region selected is indeed devoid of bright *red* stars.

Moreover, in order to verify the suitability of this field to significantly fainter limits, in July 2016 we secured deep *Ugrz* observations with the Large Binocular Cameras (LBCs) on the  $2 \times 8.4$  m Large Binocular Telescope (LBT) atop Mt. Graham, Arizona (Jansen et al. 2017b, 2019a [in prep.]). Fig. 4 shows a color composite of a portion of the full LBT/LBC images that covers the *JWST* NEP TDF and its immediate surroundings. The individual *Ugrz* mosaics for that color composite were produced following Ashcraft et al. (2018).

The faintest sources discernable with white to orange hues have  $m_{\text{AB}} \sim 26.0$ – $26.5$  mag. The effective resolution in this color composite is  $\sim 0''.95$  (FWHM). There are no bright stars within the field that NIRCam would cover in an implementation of *JWST* observations similar to those outlined in § 4 (indicated by a gray dashed circle with a radius of  $7'$ ), and there is no hint of Galactic cirrus, nor of filaments or patches of dust. In fact, the image shows a wide variety and large number of faint background galaxies, including some groups and distant clusters of galaxies (orange hues), along with a smattering of faint stars, as one would expect for a field at intermediate Galactic latitude ( $b^{\text{II}} \simeq +33.6^\circ$ ). For a detailed description of these LBT/LBC data, we refer the reader to Jansen et al. 2019a (in prep.).

### 3. DISCUSSION

#### 3.1. *The best continuously accessible survey field for JWST*

The very best field selected from our analysis of  $\sim 4 \mu\text{m}$  source penalties in the *JWST*'s northern CVZ has central coordinates of  $(\text{RA}, \text{Dec})_{\text{J2000}} = (17:22:43.12, +65:49:36.0)$ . Fig. 5a shows a more detailed map of these source penalties weighted by the inverse of the Galactic foreground reddening  $E(B-V)$  (i.e., weighted towards the regions of lowest extinction). There are adjacent good fields  $\sim 1-2'$  toward the north, east, and northwest, as well as a cluster of fields  $\sim 8'$  to the northeast, that are almost as good as this very best field in terms of both source penalty and Galactic foreground extinction. That makes this field ideal for not just a  $\sim 14'$  diameter *JWST* time-domain survey, but also for future extensions to a deep or medium-deep extragalactic survey that covers a wider area.

It may be of interest to compare  $\sim 4 \mu\text{m}$  backgrounds and source penalties within the NEP TDF with those in established deep fields like the CANDELS (Grogin et al. 2011; Koekemoer et al. 2011) GOODS-N (including the HDF-N), GOODS-S (including the HUDF), and COSMOS fields. While not continuously accessible to *JWST*, the best possible backgrounds at  $4.4 \mu\text{m}$  in the middle of their visibility windows are  $\sim 0.20, 0.19,$  and  $0.23 \text{ MJy/sr}$ , respectively, as compared to  $\sim 0.23 \text{ MJy/sr}$  for the NEP TDF<sup>2</sup>. Backgrounds corresponding to dates of observation that allow a  $180^\circ$  flip in orientation are higher ( $\sim 0.27, 0.31,$  and  $0.53 \text{ MJy/sr}$ ), while there is no restriction on date of observation for the *JWST* NEP TDF, where backgrounds are typically  $\sim 0.24 \text{ MJy/sr}$  and never higher than  $\sim 0.26 \text{ MJy/sr}$ . Source penalty values are very similar to or even slightly lower in the GOODS-S/HUDF area than in the *JWST* NEP TDF, with a similarly large choice in placement of the field center. In fact, *JWST* could center a deep  $14'$  diameter survey that would be devoid of  $4 \mu\text{m}$ -bright point sources almost anywhere within the deep portion of the fiducial CANDELS GOODS-S footprint as well as within a portion of the WFC3/ERS field (Windhorst et al. 2011). The CANDELS GOODS-N footprint contains one and is significantly encroached by four relatively bright sources, leaving only a highly constrained area free of such sources that is ideal for a deep  $14'$  diameter *JWST* survey. In that very best area, source penalty values are  $\lesssim 2\times$  higher than in the *JWST* NEP TDF.

A *time-domain* field must be accessible 365 days per year, however, which implies a location within a CVZ. In the following section we will discuss considerations that might favor particular center coordinates that are offset with respect to the best field center for *JWST*.

#### 3.2. *Other considerations*

##### 3.2.1. *VLA Radio Interferometric Observations*

Deep Karl G. Jansky Very Large Array (VLA) radio observations can be obtained most efficiently if a suitable, unresolved phase calibration source is located exactly in the center of the synthesized beam. The best  $14'$  diameter

field for *JWST* includes a  $m_{z, \text{AB}} \sim 16.9 \text{ mag}$  (SDSS; York et al. 2000) flat-spectrum quasar at  $z = 1.4429$  (Hewett & Wild 2010) with a NVSS (Condon et al. 1998) flux density of  $239.4 \pm 7.2 \text{ mJy}$  at 1.4 GHz, and (VCS5; Kovalev et al. 2007) VLBA flux densities of  $\sim 230 \text{ mJy}$  at 2.3 GHz and  $\sim 140 \text{ mJy}$  at 8.6 GHz, respectively. In the VCS5 catalog, this quasar is classified as a suitable phase calibrator that remains unresolved<sup>7</sup> at VLBA resolution, and has coordinates  $(\text{RA}, \text{Dec})_{\text{J2000}} = (17:23:14.1381, +65:47:46.178)$ , i.e.,  $\sim 2.7'$  to the southeast of the very best field center for *JWST*. VLA 3 GHz ( $\lambda = 10 \text{ cm}$ ; PI: R. Windhorst) and VLBA 5 GHz (6 cm; PI: W. Bricken) observations to  $\mu\text{Jy}$  sensitivities, centered on these coordinates, started in November 2017 and are ongoing. Fig. 4 indicates the location of the phase calibrator, and shows the footprints of these radio observations as pink dotted and dashed, and magenta dashed circles, respectively.

The ability to study variable AGN and cataclysmic events in both radio and near- to mid-infrared at similar resolutions, in order to trace the co-evolution of supermassive blackholes and their host-spheroids over cosmic time, was deemed sufficiently compelling to consider a move of the *JWST* field. The field cannot be moved over all the way to be centered on the  $z = 1.4429$  quasar, however, since that would cause a bright red star capable of saturating the NIRCcam detectors to enter the field of view, resulting in unacceptable persistence. The IDS *JWST* GTO observations of R. Windhorst as specified and implemented in APT<sup>8</sup> versions prior to 25.2.1 (2017 July 6) were therefore moved to a compromise field center of  $(\text{RA}, \text{Dec})_{\text{J2000}} = (17:23:02.55, +65:49:36.0)$ , such that the *JWST*/NIRCcam+NIRISS survey footprint would fall entirely within the VLA 3 GHz half-power beam width, and most of the NIRISS survey footprint would be encompassed by the VLBA 5 GHz half-power beam width. It is at this compromise position that ancillary ground-based near-infrared imaging in *J* and *K* were secured in 2017 with MMT/MMIRS (PI: C. Willmer) as indicated by the dark red dot-dashed square in Fig. 4. Future papers will describe and analyse these and other ancillary data (mentioned below) in detail.

##### 3.2.2. *Hubble Space Telescope observations*

UV-visible imaging with *HST* of the central  $5'$  radius portion of the *JWST* NEP TDF, plus an extension toward the south-southeast to  $r \sim 7'$ , using WFC3/UVIS (F275W) and ACS/WFC (F435W and F606W) was approved for Cycle 25 (GO-15278; PI: R. Jansen). Simultaneous *HST* guide star availability for a pattern with 8 effective field centers and 9 distinct orientations, each highly constrained to be able to make use of *HST*'s scarce near-CVZ opportunities for this field (see Jansen et al. 2018a) proved a problem at the VLA+*JWST* compromise field center. By shifting

<sup>7</sup> See, e.g., [https://gemini.gsfc.nasa.gov/results/vcs/vcs5/vcs5\\_cat.html](https://gemini.gsfc.nasa.gov/results/vcs/vcs5/vcs5_cat.html).

<sup>8</sup> See *JWST Astronomer's Proposal Tool*, APT, JWST User Documentation, 2018, STScI (Baltimore, MD); <https://jwst-docs.stsci.edu/display/JPP/JWST+Astronomers+Proposal+Tool%2C+APT>. APT is available from <http://apt.stsci.edu/>.

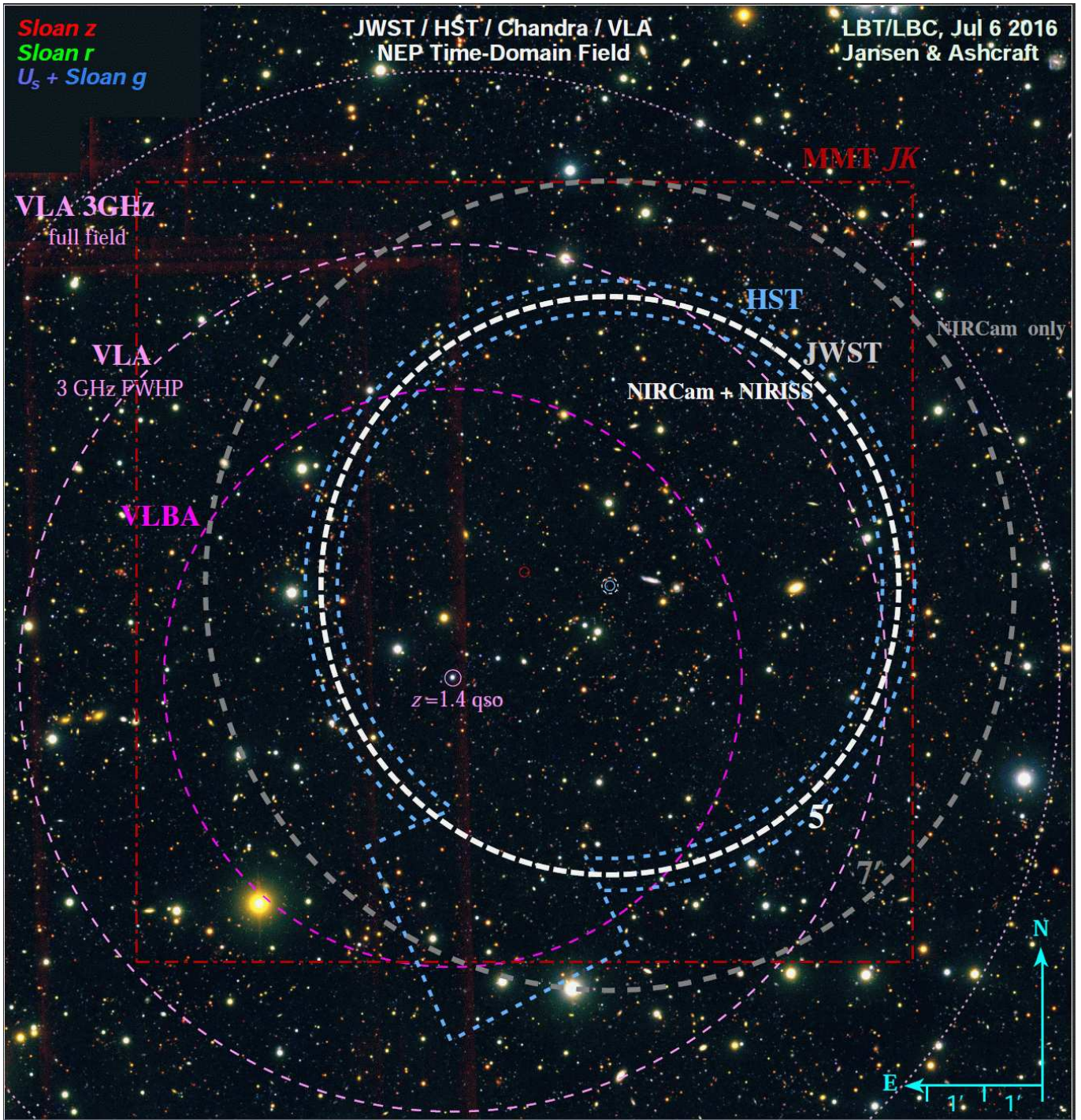


**Figure 4.** A  $19' \times 20'$   $Ugrz$  color image covering the *JWST* Time-Domain Field (TDF) and its immediate surroundings, obtained by Jansen & Ashcraft using the  $2 \times 8.4$  m Large Binocular Telescope (LBT). The depth in each of  $U$ ,  $g$ , and  $r$  exceeds  $m_{AB} = 26$  mag, while  $z$  is only slightly shallower. There are no bright stars in the NIRCam field (gray dashed circle), and the whole area has  $E(B-V) \lesssim 0.028$  mag. The red square indicates extant MMT/MMIRS  $J$  and  $K$  coverage (PI: C. Willmer), while the pale blue contour approximates our *HST* WFC3/UVIS  $F275W$  and ACS/WFC  $F435W$  and  $F606W$  coverage (PI: R. Jansen; Jansen et al. 2018a). The pink dashed and outer dotted circles indicate the half-power and full extent of our VLA 3 GHz field (PI: R. Windhorst); the magenta dashed circle corresponds to the half-power VLBA coverage at 5 GHz (PI: W. Briskin; up to  $\sim 800$  VLA-detected sources will be followed up at high angular resolution with the VLBA). The VLA/VLBA pointing center is on VCS5 (Kovalev et al. 2007) J172314.1+654746, a  $\sim 0.2$  Jy flat-spectrum quasar at  $z = 1.4429$  that remains unresolved even by the VLBA. Scheduled *Chandra*/ACIS-I X-ray observations (PI: W. Maksym) target the entire area with *JWST* and VLA coverage. This is the only clean survey region in the sky with a perfect point source radio calibrator where *JWST* can get NIRCcam  $1-5 \mu\text{m}$  imaging to 29 mag and overlapping NIRISS  $1.8-2.2 \mu\text{m}$  spectra to 28 mag at any time of the year: the ideal time-domain field. The brightest yellow star prevents the *JWST* field center from precisely coinciding with the radio field center.

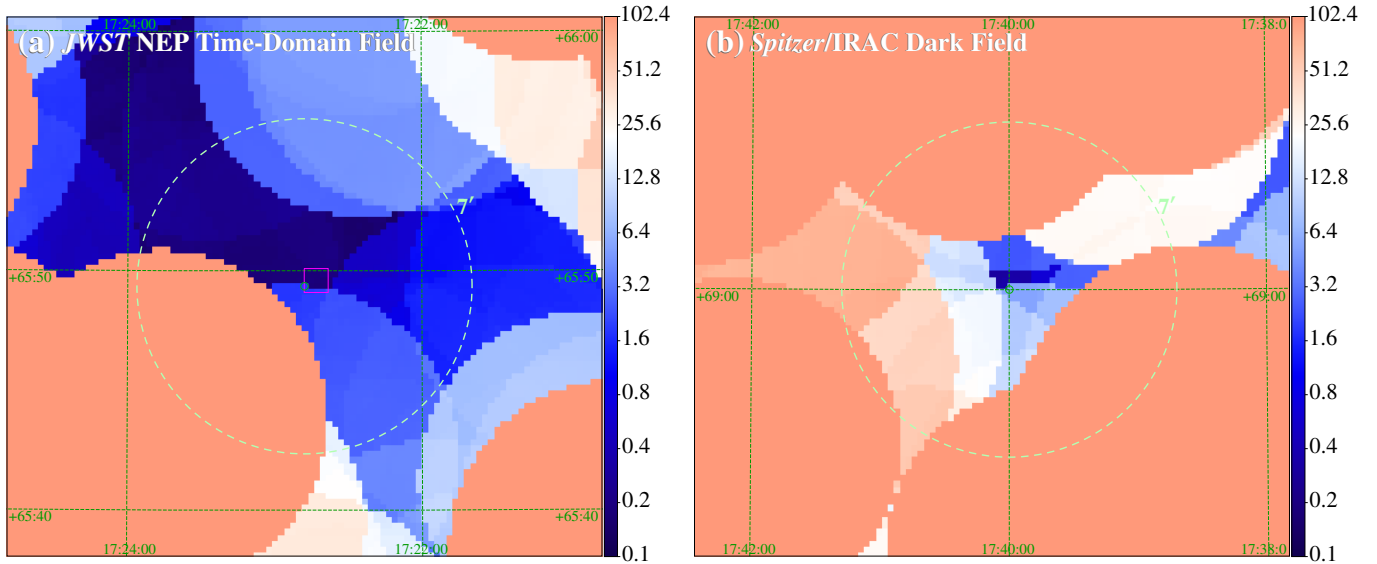


**Figure 5.** Comparison of  $18' \times 18'$  maps of the bright source penalties of Fig. 3a multiplied by the Galactic foreground reddening of Fig. 2a for [a] the *JWST* NEP TDF, and [b] the *Spitzer*/IRAC Dark Field (IDF). For a circular viewport with a diameter of  $14'$ , a step size of  $15''$ , and source penalties that decrease by a factor 10 per unit magnitude, the value at the center of the best survey field for *JWST* (indicated by the magenta square) is  $\sim 0.18$ , compared to  $\sim 0.30$  near the center of the IDF. While that difference is less than a factor 2, the most striking feature of the comparison is that there is a much wider area around the NEP TDF that is nearly as good as the NEP TDF proper, i.e., there is room for a survey that is much wider than can be accommodated at or near the IDF without running into bright stars. In fact, the dashed circle in panel (a) is shifted slightly east and south with respect to the very best field center, in order to accommodate *HST* guide star solutions at multiple roll angles (see § 3.2.2).

the field center  $90''$  west (i.e., back in the direction toward the objectively selected best field center) and  $14''$  south, a viable solution was found, however, for  $(\text{RA}, \text{Dec})_{\text{J2000}} = (17:22:47.896, +65:47:21.54)$ , as indicated in Fig. 4 by a small pale blue circle. This field center was subsequently adopted (small dashed white circle) for the IDS *JWST* GTO observations of R. Windhorst (indicated by the white and grey dashed circles with radii of  $5'$  and  $7'$ , respectively) and H. Hammel as implemented in APT version 25.4.2, and made public by the *JWST* Project on Feb. 6, 2018, making it the *de facto* coordinates of the *JWST* NEP TDF. Since the VLA still has significant sensitivity beyond its half-power beam width, all of the *JWST*/NIRCam observations in the NEP TDF will still have coverage at 3 GHz.

### 3.2.3. Other proposed, approved, and scheduled observations

These *de facto* coordinates of the *JWST* NEP TDF were also adopted for proposed *JWST* ERS observations in this field (MIRI+NIRCam imaging: H. Messias et al.; NIRISS wide-field slitless spectroscopy: S. Malhotra et al.), as well as for *Chandra*/ACIS-I X-ray imaging in progress (Cycle 19 program 19900666; PI: W. Maksym) and approved (time-domain monitoring Cycle 20+21 program 20900658; PI: W. Maksym), for IRAM 30m/NIKA2 mm-wave observations in progress (PI: S. Cohen), for approved and proposed JCMT/SCUBA2 (PI: I. Smail, M. Im), LOFAR (PI: P. Best), and 4.2 m WHT/WEAVE (PI: K. Duncan) observations, for MMT/Binospec multi-object spectroscopy and MMT/MMIRS Y (some *H*) near-IR imaging in hand (PI:

C. Willmer), and proposed *Spitzer*/IRAC (PI: M. Ashby) imaging, and SMA (PI: G. Fazio) sub-mm interferometry. The field and its wider surroundings have also been targeted with Subaru/HSC in five filters (*g, i, z, NB<sub>816</sub>, NB<sub>921</sub>*) as part of the Hawaii EROsita Ecliptic-pole Survey (HEROES; PI: G. Hasinger), and with the J-PAS (Benítez et al. 2014) PathFinder for spectrophotometric narrow-band imaging (*u<sub>griz</sub>* observations with HiPERCAM on the 10 m GTC (PI: V. Dhillon) are also proposed.

### 3.3. A critical comparison of the *JWST* NEP TDF and the *Spitzer*/IRAC Dark Field

Every two to three weeks throughout its mission, *Spitzer*/IRAC (Fazio et al. 2004) observations were made of a field near the NEP and centered at  $(\text{RA}, \text{Dec})_{\text{J2000}} = (17:40:00, +69:00:00)$ , the IRAC Dark Field (IDF), for the purpose of dark and bias calibration of its detectors. This field is also located well within the northern *JWST* CVZ, and its original selection also aimed to target an empty patch of sky, avoiding bright stars and extended galaxies. Over time, this has resulted in the deepest extant near-IR extragalactic survey field, with a  $\sim 15$  year baseline for time-domain studies in its shortest wavelength bandpasses. The field was also augmented with deep observations at other wavelengths from X-ray through far-infrared (Krick et al. 2009). The clean portion of the  $\sim 20'$  diameter IDF to the depths reached by *JWST*/NIRCam is much smaller, however, and of the order of no more than  $r \sim 7'$ , as can be seen in Fig. 6b.



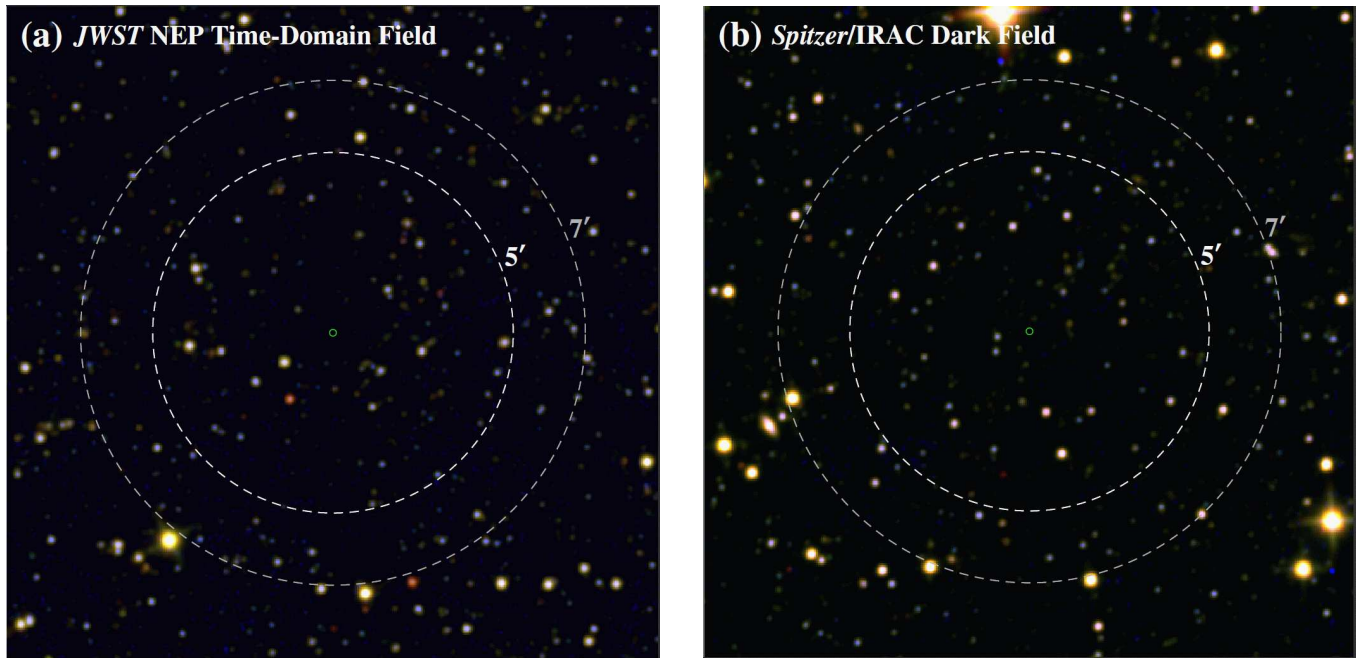


**Figure 6.** Comparison of near-infrared color composites of [a] the selected *JWST* NEP Time-Domain Field, and [b] the *Spitzer*/IRAC Dark Field. In each  $18' \times 18'$  image, 2MASS *J*, *WISE*  $3.4 \mu\text{m}$ , and *WISE*  $4.6 \mu\text{m}$  images are shown at  $\sim 6''.4$  resolution (FWHM) in blue, green, and red hues. Dashed white and grey circles have radii of  $5'$  and  $7'$ , respectively. While the central portion of the IDF is nearly as free of bright sources as the NEP TDF, the latter can be moved or expanded a few arcminutes up (north), and then left (east) or right without including additional bright sources.

Indeed, Fig. 3a shows that on scales of  $14'$ , the IDF does not stand out as an optimal field for *JWST*. Fig. 5b emphasizes that, while (weighted) source penalties in  $14'$  diameter circular viewports are only slightly higher in the IDF than in the very best area selected for the *JWST* Time-Domain Field, the latter field can accommodate a deep *JWST* survey over a much wider area. Figs. 6a and 6b compare the TDF and IDF in a near-infrared color composite that directly shows the low densities of bright sources within and encroachment of bright sources around the periphery of the IDF, while the TDF has ample room to expand to the north, northeast, and west. For reference, the brightest star encroaching the IDF toward the north has  $m_{K,AB} = 7.69$  mag, whereas the brightest star near the TDF toward the southeast has  $m_{K,AB} = 10.73$  mag. Also when comparing the mean (median)  $\sim 2 \mu\text{m}$  brightness of 2MASS-detected stars within the cleanest central areas ( $r \leq 7'$ ) of the IDF and TDF, we find that the TDF fares slightly better:  $\langle m_{K,AB} \rangle = 16.17$  (16.65) for the IDF versus 16.65 (16.92) mag for the TDF. The negative impact due to persistence effects on deep *JWST* surveys is therefore expected to be slightly reduced in the TDF compared to the IDF.

While well matched to the field of view of the *Spitzer*/IRAC detectors, the clean portion of the IDF is too small for our intended deep *JWST* imaging and slitless spectroscopic observations, which require a clean area of at least  $14'$  diameter.

### 3.4. The Promise of Parallel Observations

Parallel science observations with *JWST* were originally neither planned, nor permitted. In support of efficient on-orbit instrument calibration after launch, “parallel instrument calibrations” were, however, to be implemented (e.g., Gardner et al. 2006). In 2015, the *JWST* Project and STScI decided that parallel *science* observations ought to be implemented as well, in order to maximize the scientific return of *JWST*. This is especially important in view of the finite lifetime of *JWST* —as set by its finite supply of fuel for station keeping and momentum control— of 5 (required), 10 (expected), or at most 14 (goal) years, which is much shorter than that of *HST* (28 years and counting).

During most of its operational lifetime, the depth and areal efficiency of *HST* grism spectroscopic surveys has added valuable low-resolution spectra to many of the deepest *HST* imaging surveys, which was essential to measure the redshifts and characterize the properties of faint objects. Prime examples of such *HST* grism surveys are the Grism ACS Project for Extragalactic Science (GRAPES; e.g., Pirzkal et al. 2004; Pasquali et al. 2006), the ACS Probing Evolution and Reionization Spectroscopically (PEARS; e.g., Pirzkal et al. 2013; Straughn et al. 2008, 2009), the WFC3 grism survey (3DHST; e.g., Momcheva et al. 2016), the WFC3 Infrared Spectroscopic Parallel survey (WISP; e.g., Atek et al. 2010), the Grism Lens-Amplified Survey from Space (GLASS; e.g., Treu et al. 2015; Schmidt et al. 2014), and the Faint Infrared Grism Survey (FIGS; e.g., Pirzkal et al. 2017;

Larson et al. 2018). We note that of these only WISP was an *HST* parallel survey. The others targeted areas with pre-existing deep imaging, and obtained grism spectroscopy with the primary instrument, while adding imaging parallels. Due to *HST*'s extraordinary longevity, grism spectroscopy and direct imaging surveys could be completed in a largely separate manner. For *JWST*, with its much shorter expected life-time, direct imaging and slitless grism spectra (NIRISS; especially for blind emission-line searches) or multi-object slit-spectra (NIRSpec; targeted spectroscopy to the faintest limits) must be done *concurrently* to the largest extent possible. Just like for *HST*, we expect that *JWST* NIRISS grism and NIRSpec multi-object spectroscopy will constitute an essential complement to NIRC*am* imaging observations to even fainter limits ( $m_{AB} \gtrsim 27$  mag). Since we anticipate that GO proposers will revisit the *JWST* NEP Time-Domain Field many times, the coordinates of even very faint objects will generally be known in time to allow targeted spectroscopy and imaging in parallel.

### 3.5. Estimated Source Counts and Number of Variable Objects in the *JWST* NEP Time-Domain Field

Deep *HST* observations can inform our expectations for the near-IR source counts within the *JWST* NEP TDF. To  $m_{AB} \sim 29$  mag, the HUDF  $1.6 \mu\text{m}$  (*H*); as most representative of *JWST*) counts show  $3.5 \times 10^5$  objects per 0.5 mag interval per square degree (Fig. 12 of Windhorst et al. 2011). The  $1.6 \mu\text{m}$ -counts over the  $20 \lesssim m_{AB} \lesssim 29$  mag range show a sub-converging slope of  $0.213 \text{ mag dex}^{-1}$  (see also Driver et al. 2016). Therefore, the *total* integrated galaxy counts to  $m_{AB} \lesssim 29$  mag are expected to reach  $\sim 1.79 \times 10^6$  objects per  $\text{deg}^2$ . The number of Galactic stars at the NEP to the same flux limits is only  $(0.4\text{--}0.9) \times 10^4$  per  $\text{deg}^2$  (Ryan et al. 2011; Ryan & Reid 2016), which is still a  $\sim 5\text{--}10 \times$  larger density of stars than seen in the *HST* surveys summarized by Windhorst et al. (2011) at high Galactic latitude.

Similarly, given typical faint radio source counts (Condon et al. 2012; Vernstrom et al. 2014; Windhorst et al. 1985, 1993; Hopkins et al. 2000), we expect that a VLA survey that reaches a depth of  $5 \mu\text{Jy}$  ( $5\sigma$ ) at 3 GHz would detect a *total* of  $\sim 2.2 \times 10^4$  sources per square degree. This calculation assumes that the normalized differential source count slope continues to be as steep as  $-1.7$  at  $\mu\text{Jy}$  levels (Condon et al. 2012), and a spectral index between 3 and 1.4 GHz for these sources of about 0.4, following the trends seen at somewhat brighter levels between 1.4, 5.0, and 8.4 GHz (Windhorst et al. 1993). The models of Hopkins et al. (2000) indicate that somewhat more than half of the radio sources seen at  $\mu\text{Jy}$  levels will turn out to be starburst galaxies or vigorously star forming regions within galaxies, while the remainder are caused by weak AGN. The latter would appear as unresolved radio sources. The exact ratio of starbursts and AGN will of course await VLBA observations at  $\mu\text{Jy}$  levels and the *HST* + *JWST* images and grism spectra.

Both VLA 3 GHz and *Chandra* X-ray coverage will be available for the *JWST* NEP TDF, as well as significant partial coverage with *JWST*/NIRISS grism and *HST* UV-Visible

imaging observations. If we consider the  $\sim 153.9 \text{ arcmin}^2$  and  $\sim 71.8 \text{ arcmin}^2$  areas of the full  $14'$  diameter *JWST* NEP TDF and of the footprint that will be sampled in our initial *JWST* NIRC*am* GTO observations (§ 4), then we estimate a total number of faint galaxies (stars) detected to  $m_{AB} \sim 29$  mag of  $\sim 7.65 \times 10^4$  (170–385) and  $\sim 3.57 \times 10^4$  (80–180), respectively. In the same *JWST* NEP TDF areas, we expect to detect a total of  $\sim 940$  and  $\sim 440$  faint 3 GHz radio sources to  $5 \mu\text{Jy}$ , almost half of which will be weak radio-selected AGN.

In an optical search for weak AGN, Sarajedini et al. (2011) and Cohen et al. (2006) monitored faint galaxies at  $z \simeq 0.5\text{--}4$  with *HST* WFPC2 or ACS/WFC at visible (restframe UV) wavelengths on timescales of weeks to months (i.e., about a week to a month in the restframe at the median redshift of  $z \sim 2$  of the sample). These studies find that on such timescales typically  $\sim 1\%$  of the faint optically selected galaxies at a given redshift shows significant evidence for variability in their cores (45 out of 4644 galaxies in the HUDF), about half of which are associated with either faint X-ray sources or mid-IR power-law emission (Sarajedini et al. 2011). That paper reports, moreover, that a quarter of X-ray selected AGN are optical variables, and that this percentage increases with decreasing hardness ratio of the X-ray emission. At radio wavelengths, Ofek & Frail (2011) found in a NVSS–FIRST comparison that 0.1% of the unconfused FIRST sources in a mJy sample were variable. (Oort & Windhorst 1985) studied variability in a deeper sample of sub-mJy radio sources by comparing deep Westerbork and VLA maps of the same region in the Lynx 2 field on timescales of a month to a year. They found that  $\lesssim 2\%$  of the sub-mJy sources showed variability on both timescales.

Conservatively, within the full *JWST* NEP TDF and within the GTO-sampled portion thereof, we therefore estimate  $\gtrsim 730$  and  $\gtrsim 340$  galaxies detected to  $m_{AB} \sim 29$  mag at rest-frame optical wavelengths to vary in repeat observations with *JWST*/NIRC*am* on time-scales of weeks to years. We expect at least  $\sim 0.5\%$  of the field galaxies in the same areas to be detected at  $\mu\text{Jy}$  levels with the VLA, and confirmed with VLBA observations to be AGN (i.e.,  $\gtrsim 380$  and  $\gtrsim 175$  in total). Starburst dominated  $\mu\text{Jy}$  radio sources should be easily recognized from the 8-band *JWST* photometry and grism spectra, and are expected to appear resolved in the VLBA observations, at least partially resolved in the shorter-wavelength near-IR *JWST* filters, and mostly non-varying at radio and rest-frame visible–near-IR wavelengths, although a subset of dust-obscured ULIRGs may be found to vary at mid–far-IR wavelengths on time-scales of months to years due to their extremely high SN rates (Yan et al. 2018).

Since any variable emission from weak AGN comes from different regions around the accretion disk at radio, near–mid-IR, optical, and X-ray wavelengths, the exact fraction of variable objects at each of these wavelengths depends on the relative depth and time-sampling of each of these data sets and on the physical timescales involved in each of these wavelength regimes. With a sufficient number of epochs and sufficient depth from radio to X-rays, we hope that the *JWST*

NEP TDF will provide the database to begin to address these questions, including how large a fraction of weak AGN (variable or not) are seen in common between the radio, near-mid-IR, optical, and X-ray studies.

#### 4. POSSIBLE IMPLEMENTATIONS

Inspired by the very successful combination of *HST* direct imaging and grism spectroscopy, and in the spirit of the 3DHST, GRAPES, PEARS, FIGS, GLASS, and WISP *HST* grism surveys, we aim to find a *JWST* survey strategy that allows securing *both* primary NIRC*am* imaging and parallel NIRISS grism observations in the *JWST* NEP TDF as part of a *single* observing program, while maximizing both the overall survey area and the area of overlap between imaging and grism spectra. We consider two possible implementations — for the purpose of multi-wavelength 0.8–5.0  $\mu\text{m}$  object characterization with or without a time-domain component—, with an eventual goal of contiguous coverage of an area of  $\sim 153.9 \text{ arcmin}^2$ , the area of a circular field with a diameter of  $14'$ .

##### 4.1. A ‘Unit Visit’ of NIRC*am* and NIRISS Observations

After some experimentation with notional layouts and with supported observation descriptions in APT, one natural pattern for a *unit visit*<sup>9</sup> emerged: it results in two, offset, contiguous areas covered by NIRC*am* and NIRISS in parallel, and maximizes the potential overlap of the footprints of the two instruments. That pattern, shown in Fig. 7*a*, consists of a 2-point mosaic with a pointing offset approximately equal to the width of a NIRISS detector projected onto the sky, and is specified in APT as a  $2 \times 1$  (columns  $\times$  rows) mosaic with an overlap of 57% of the two NIRC*am* footprints (i.e., both modules combined). In combination with a standard  $\geq 3$ -point INTRAMODULE NIRC*am* dither at each mosaic pointing, this unit pattern will fill both the large intra-module gap and the small gaps between the four individual detectors in the SW channels of each NIRC*am* module. By specifying an offset of  $(190''0, -105''0)$ , the unit pattern becomes rotationally symmetric around the desired nominal field center (indicated by the black dot in Fig. 7*a*), with maximal overlap between the NIRISS and NIRC*am* coverages after rotation over  $180^\circ$ .

This unit pattern also results in an area of overlap between the coverage of NIRC*am* Modules A and B ( $\sim 3.6 \text{ arcmin}^2$ ), with an effective exposure time up to twice the nominal one (see Table. 1 and the dark shaded region in Fig. 7*a*). This overlap allows photometric and astrometric cross-calibration between the two modules, verification of systematics near the detection limit in areas with nominal depth, as well as time-domain sampling on time-scales of  $\sim 0.4$ – $1.0$  hr (assuming a medium-deep NIRC*am* imaging survey to  $m_{\text{AB}} \sim 29$  mag in 8 filters with coordinated parallel NIRISS grism obser-

vations, and all the operational constraints imposed by the observatory). An additional benefit as originally envisioned was that this pattern would provide repeat sampling on time-scales of several hours for the area of overlap between the two NIRC*am* modules. This required cycling through each of the filters at a given pointing before executing the offset in the mosaic. Overriding concerns for the longevity of the (large) NIRC*am* filter wheels, however, disallow such cycling and force all pointing offsets in a visit to be executed before moving to the next filter.

##### 4.2. An IDS GTO Program to Start Object Characterization and Time-Domain Monitoring of the JWST NEP TDF

Building on this unit visit pattern, program GTO-1176 (PI: R. Windhorst) will map an area of  $\sim 71.8 \text{ arcmin}^2$  in the *JWST* NEP TDF in 8 filters that span the 0.8–5.0  $\mu\text{m}$  wavelength range of NIRC*am*. The nominal 3-dither depth of  $m_{\text{AB}} \sim 29$  mag ( $5\sigma$ ) is met or exceeded for a total area of  $\sim 49.3 \text{ arcmin}^2$ . The GTO coverage, shown in Fig. 7*b*, consists of four distinct ‘spokes’, each oriented  $90^\circ$  apart, and is charged  $\sim 47$  hrs ( $4 \times 11.7$  hrs) of calendar time. Since the *JWST* CVZs are the *only* place in the sky where *JWST* can revisit a target with an aperture orientation rotated over  $180^\circ$  with respect to a prior visit — without a significant penalty in the form of an increased Zodiacal foreground brightness —, this is the *only* place in the sky where coordinated parallel observations with a second instrument (e.g., NIRISS, MIRI) can be made to almost fully overlap such prior NIRC*am* observations, and vice versa. For the Windhorst IDS GTO program, the combination of 1.8–2.2  $\mu\text{m}$  NIRISS wide-field slitless spectroscopy and NIRC*am* imaging for the purpose of source characterization was deemed particularly powerful. The areas where NIRISS and NIRC*am* coverage overlap appear in light blue to purplish hues within the white dashed inner circle of radius  $5'$  in Fig. 7*b*. The direct images bracketing the dispersed NIRISS grism exposures reach to  $> 29$  mag as well, and allow time-domain monitoring of an area of  $\sim 45.0 \text{ arcmin}^2$  (of which  $\sim 33.6 \text{ arcmin}^2$  at nominal

**Table 1.** Areal coverage vs. relative depth for the adopted Unit Visit, a  $2 \times 1$  mosaic with a 3-point NIRC*am* INTRAMODULE dither

Instrument	Depth [ $N_{\text{int}}$ ]	Area [ $\text{arcmin}^2$ ]	Depth [ $N_{\text{int}}$ ]	Area [ $\text{arcmin}^2$ ]
NIRC <i>am</i>	1 <sup>a</sup>	2.240	$>0$	18.335
	2	3.951	$>1$	16.095
	3 <sup>b</sup>	8.524	$>2^c$	12.145
	4	0.926	$>3$	3.621
	5	1.416	$>4$	2.695
	6	1.279	$>5$	1.279
NIRISS	1 <sup>a</sup>	1.666	$>0$	11.580
	2	1.572	$>1$	9.914
	3 <sup>b</sup>	8.212	$>2^c$	8.342
	4	0.130	$>3$	0.130

Notes: (a) at single-exposure depth, some unrecoverable image defects will persist, and the PSF will be poorly sampled; (b) nominal, 3-dither depth is reached; (c) nominal depth is reached or exceeded.

<sup>9</sup> With *unit visit* we mean a sequence of pointings and dithers executed within a single *JWST* visit for a specified set of optical elements.

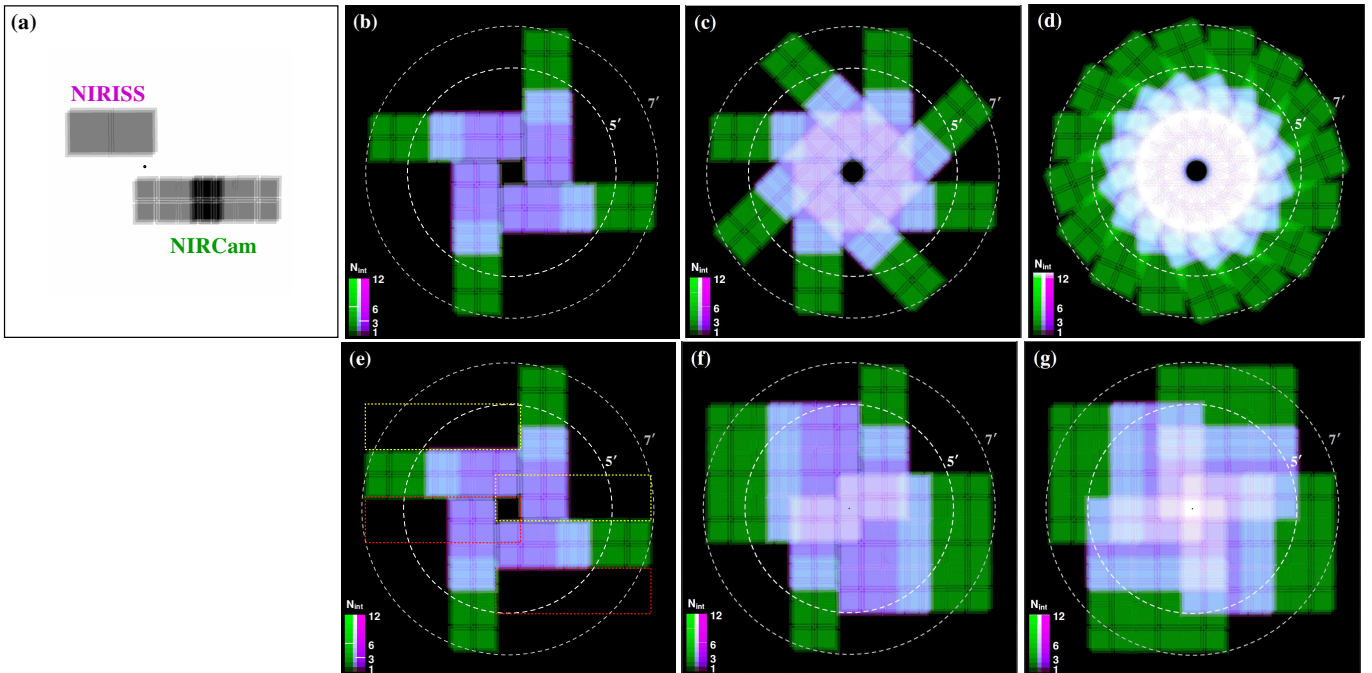


**Figure 7.**  $15' \times 15'$  exposure maps of [a] the *unit visit* described in § 4.1, resulting in two, offset, contiguous areas covered by NIRCams and NIRISS. The nominal *JWST* pointing center is indicated by a black dot. [b] a 4-spoke design like that adopted in GTO program 1176 of the basic pattern of panel (a), where the spokes have orientations that differ by  $90^\circ$  on the sky. Offsets are such that NIRCams covers the NIRISS observations taken 180 days ( $\Delta\text{PA} = 180^\circ$ ) earlier or later, and NIRISS will sample a large portion of the area imaged by NIRCams. [c and d] Additional orientations ( $\Delta\text{PA} = 45^\circ$  and  $\pm 22.5^\circ$ , respectively) of similar pairs of spokes will increase the total area covered, as well as the area sampled at multiple epochs. [e–g] For the purpose of multi-filter object characterization (as opposed to time-domain monitoring of objects already characterized), a more efficient design could build directly on the four orientations of GTO 1176, maximizing the contiguous surface area covered per unit calendar time. The contiguous area of panel (g) is nearly equivalent to the  $\sim 153.9 \text{ arcmin}^2$  of a circular area with a radius of  $7'$ . The actual orientation of these patterns on the sky, shown here aligned with the cardinal axes, will depend on the *JWST* launch date.

depth or better) on time-scales of 180 days when compared to the corresponding NIRCams  $2.0 \mu\text{m}$  images.

GO extensions of the GTO pattern with an additional four spokes with the pattern rotated over  $45^\circ$ , as shown in Fig. 7c, would cover  $\sim 114.4 \text{ arcmin}^2$ , while a further eight spokes at orientations of  $\Delta\text{PA} = \pm 22.5^\circ$  (Fig. 7d) would approach our  $153.9 \text{ arcmin}^2$  goal. Such extensions with similar pairs of spokes will not only increase the total areal coverage, but also the area sampled at multiple epochs with increasingly dense time-domain sampling. Furthermore, assuming NIRISS is used in parallel to NIRCams for grism spectroscopy also in such GO programs, the number of distinct orientations aids in disentangling spectra contaminated by signal from neighboring objects within the field of view (e.g., Ryan et al. 2018).

Once source characterization is available, the same unit visit pattern can be used for efficient time-domain monitoring (to the same flux limits) of sources that either move or vary in brightness. For monitoring, one would need only one SW (e.g., F200W) and one LW (e.g., F356W) NIRCams filter, observed simultaneously, and direct imaging (e.g., F200W) with NIRISS in parallel.

### 4.3. Efficient Areal Mapping for Object Characterization

When object characterization and time-domain monitoring are considered as two entirely separate goals, an alter-

native, more efficient design using the same unit visit pattern is possible for object characterization. It can cover  $\sim 150\text{--}155 \text{ arcmin}^2$  in the *JWST* NEP TDF in 8 NIRCams filters to the same depth of  $m_{\text{AB}} \sim 29$  mag, with the same parallel NIRISS  $1.8\text{--}2.2 \mu\text{m}$  grism spectroscopy and F200W direct imaging. This design is illustrated in Fig. 7e–g. Whereas the survey strategy of § 4.2 (Fig. 7b–d) rotates the pattern to leverage the year-round accessibility of the field for time-domain science, it leaves a hole in the coverage at the nominal field center. An approach using offsets with respect to the spokes of GTO-1176, and more constrained scheduling—either within a few days from the GTO visits, or a full year later—could cover a contiguous area that is nearly equivalent to the  $\sim 153.9 \text{ arcmin}^2$  of a circular area with a diameter of  $14'$ , while leaving no such hole. In fact, the central  $\sim 0.5$ ,  $\sim 4.2$ , and  $\sim 26.3 \text{ arcmin}^2$  would be sampled at 4, 3, and 2 times the nominal depth, respectively. The coverage shown in Fig. 7g would require (APT25.4.4) under 93 hrs of calendar time in addition to the GTO observations (as compared to an additional  $\sim 141$  hrs for the coverage of Fig. 7d).

While the main aim of this design is to secure source characterization in the NEP TDF early-on in the *JWST* mission, even here there are significant areas of overlap between the offset spokes that would provide time-domain sampling on

time-scales of  $\lesssim 3$  days and of multiples of  $\sim 90$  days (up to  $\sim 1$  yr).

## 5. SUMMARY

We described the selection of a new extragalactic survey field optimized for time-domain science with *JWST*. It is located within *JWST*'s northern continuous viewing zone and is centered at (RA, Dec)<sub>J2000</sub> = (17:22:47.896, +65:49:21.54). This *JWST* North Ecliptic Pole (NEP) Time-Domain Field (TDF) is the *only*  $\gtrsim 14'$  diameter area where *JWST* can observe a clean extragalactic survey field at any time of the year and at arbitrary orientation, while leveraging *JWST*'s capability to perform parallel science observations. The NEP TDF will be targeted by *JWST* GTO program 1176, has a rich and growing complement of multi-wavelength ancillary ground- and space-based observations, and has an unmatched potential as a *JWST* time-domain *community field*. We estimated the number of sources expected to be detectable to  $m_{AB} \sim 29$  mag with *JWST* in the near-IR and to  $\mu\text{Jy}$  flux levels in deep VLA 3–5 GHz radio observations, as well as the subsets thereof expected to show significant variability. Last, we presented an efficient unit visit, comprising primary NIRC*am* imaging and parallel NIRISS slitless grism spectroscopy, with which observing programs can be designed for wide-area source characterization and time-domain monitoring. We encourage *JWST* GO proposers to adopt this efficient mode of observations for future *JWST* cycles, and hope that the NEP TDF will become one of *JWST*'s community fields.

**Acknowledgements.** The authors acknowledge support from *JWST* grants NAGS-12460, NNX14AN10G, and 80NSSC18K0200 from the National Aeronautics and Space Administration (NASA) Goddard Space Flight Center (GSFC), and from grant HST-GO-15278.001-A from the Space Telescope Science Institute, which is operated by the Association of Universities for Research in Astronomy, Inc. (AURA) under NASA contract NAS 5-26555. We are grateful to the *HST* Project at NASA GSFC and STScI for implementing *JWST* parallels also for science observations.

We thank Teresa Ashcraft for the preliminary reduction of the LBT/LBC data used for Fig. 4; Christopher Willmer for sharing his Fortran code to compute the exposure map shown in Fig. 7*a*; Russell Ryan for kindly providing number counts of Galactic stars computed specifically for the *JWST* NEP TDF; and Seth Cohen for suggesting a pinwheel pattern for *JWST* NIRC*am*+NIRISS observations. We thank Walter Briskin, James Condon, Bill Cotton, Ken Kellermann, Rick Perley, Peter Maksym, Norman Grogin, Patricia Royle, Anton Koekemoer, Steven Rodney, Adam Riess, Lou Strolger, Nimish Hathi, Michael Rutkowski, Chris Conselice, Simon Driver, Steven Finkelstein, Brenda Frye, Haojing Yan, Dan Coe, Madeline Marshall, Victoria Jones, Cameron White, Günther Hasinger, Christopher Waters, Esther Hu, Giovanni Fazio, Matt Ashby, Heidi Hammel, Stefanie Milam, Chad Trujillo, Hugo Messias, Sangeeta Malhotra, Ian Smail, Myungshin Im, Ken Duncan, Justin Roberts-Pierel, Andrea

Ferrara, Stephen Wilkins, Michelle Edwards, Volker Tolls, Mehmet Alpaslan, Linhua Jiang, Patrick Kelly, Nor Pirzkal, Martin Ward, Jennifer Patience, Michael Line, Silvia Bonoli, Renato Dupke, Vik Dhillon, and Michele Bannister for useful discussions and (proposals for) ancillary observations in the *JWST* NEP TDF, and/or for comments on the manuscript, and Neill Reid, Ken Sembach, John Mather, and Eric Smith for inspiring us to develop this field as a *JWST* Community Field. We thank the anonymous referee for helpful comments and suggestions that improved this paper.

This publication used data products from *WISE*, which is a joint project of the University of California, Los Angeles, and the Jet Propulsion Laboratory (JPL)/California Institute of Technology (Caltech), funded by NASA. We used Atlas Images from the Two Micron All Sky Survey (2MASS), a joint project of the University of Massachusetts and the Infrared Processing and Analysis Center (IPAC)/Caltech, funded by NASA and the National Science Foundation (NSF). We also used data products from the Sloan Digital Sky Survey (SDSS), funded by the Alfred P. Sloan Foundation, the Participating Institutions, NASA, NSF, the U.S. Department of Energy, the Japanese Monbukagakusho, and the Max Planck Society. The SDSS is managed by the Astrophysical Research Consortium (ARC) for the Participating Institutions: The University of Chicago, Fermilab, the Institute for Advanced Study, the Japan Participation Group, The Johns Hopkins University, Los Alamos National Laboratory, the Max-Planck-Institutes for Astronomy (MPIA) and Astrophysics (MPA), New Mexico State University, University of Pittsburgh, Princeton University, the U.S. Naval Observatory, and the University of Washington. This research has made use of the NASA/IPAC Infrared Science Archive (IRSA) and NASA/IPAC Extragalactic Database (NED), which are operated by JPL/Caltech under contract with NASA.

Based in part on observations (PI: R.A. Jansen) made with the Large Binocular Telescope (LBT). The LBT is an international collaboration among institutions in the United States, Italy, and Germany. LBT Corporation partners are: The University of Arizona on behalf of the Arizona university system; Istituto Nazionale di Astrofisica, Italy; LBT Beteiligungsgesellschaft, Germany, representing the Max-Planck Society, the Astrophysical Institute Potsdam, and Heidelberg University; The Ohio State University; and The Research Corporation, on behalf of the Universities of Notre Dame, of Minnesota and of Virginia.

We used Montage (Laity et al. 2005; Jacob et al. 2009), funded by NSF and by NASA's Earth Science Technology Office, Computation Technologies Project, under Cooperative Agreement between NASA and Caltech, and maintained by the NASA/IPAC Infrared Science Archive. Montage includes an adaptation of the MOPEX algorithm developed at the Spitzer Science Center, and software developed by IPAC for the US National Virtual Observatory, which is sponsored by NSF. We used IRAF (Tody 1986, 1993), a general purpose software system for the reduction and analysis of astronomical data, which is written and distributed by the National Optical Astronomy Observatories, which are operated by

AURA under cooperative agreement with NSF. Images and color composites were rendered using SAOImage DS9 (Joye & Mandel 2003), developed by the Smithsonian Astrophysical Observatory, with funding from the Chandra X-ray Science Center, the High Energy Astrophysics Science Archive Center, and the JWST Mission office at Space Telescope Science Institute.

This research has made use of NASA's Astrophysics Data System (ADS) bibliographic services (Kurtz et al. 2000).

*Software:* (C)FITSIO, DS9, IDL, IRAF, Montage, Super-Mongo, SCAMP, SWARP; Fortran77 code and utilities written by the lead author (narg/arg, myfixnan, select, mkmask, listpix)

*Facilities:* Large Binocular Telescope (Large Binocular Cameras); Two Micron All Sky Survey; Wide-field Infrared Survey Explorer

## REFERENCES

- Artigau, É., Bouchard, S., Doyon, R., & Lafrenière, D. 2009, *ApJ* 701, 1534
- Ashcraft, T.A., Windhorst, R.A., Jansen, R.A., et al. 2018, *PASP* 130, 064102
- Atek, H., Malkan, M., McCarthy, P., et al. 2010, *ApJ* 723, 104
- Benítez, N., Dupke, R., Moles, R., et al. 2014, *J-PAS: The Javalambre - Physics of the Accelerated Universe Astrophysical Survey* "Red Book", arXiv:1403.5237
- Bertin, E., & Arnouts, S. 1996, *A&AS* 117, 393
- Buenzli, E., Apai, D., Radigan, J. et al. 2014, *ApJ* 782, 77
- Catalán, S., Napiwotzki, R., Hodgkin, S., et al. 2013, *ASP Conf. Ser.* 469, 235
- Cohen, S.H., Ryan, R.E., Jr., Straughn, A.N., et al. 2006, *ApJ* 639, 731
- Condon, J.J., Cotton, W.D., Fomalont, E.B., et al. 2012, *ApJ* 758, 23
- Condon, J.J., Cotton, W.D., Greisen, E.W., et al. 1998, *AJ* 115, 1693
- Driver, S.P., Andrews, S.K., Davies, L.J., et al. 2016, *ApJ* 827, 108
- Fazio, G.G., Hora, J.L., Allen, L.E., et al. 2004, *ApJS* 154, 10
- Gal-Yam, A. 2012, *Science* 337, 927
- Gardner, J.P., Mather, J.C., Clampin, M., et al. 2006, *Space Science Reviews* 123, 485
- Gehrels, N., Spergel, D., and the *WFIRST* SDT and Project 2015, *J.Ph.Conf.Ser.* 610, 012007
- Graur, O., Rodney, S.A., Maoz, D., et al. 2014, *ApJ* 783, 28
- Greene, T., Beichman, C., Gully-Santiago, M., et al. 2010, *Proc. SPIE* 7731, 0C
- Grogin, N.A., Kocevski, D.D., Faber, S.M., et al. 2011, *ApJS* 197, 35
- Harris, H.C., Munn, J.A., Kilic, M. et al. 2006, *AJ* 131, 571
- Hewett, P.C., & Wild, V. 2010, *MNRAS* 405, 2302
- Hopkins, A., Windhorst, R.A., Cram, L., & Ekers, R. 2000, *ExA* 10, 419
- Horner, S., Rieke, M., and the NIRCcam Team 2004, *Proc. SPIE* 5487, 628
- Ivezić, Ž. 2014, *AAS* 223, 31703
- Jacob, J.C., Katz, D.S., Berriman, G.B., et al. 2009, *IJCSE*, Vol.4 (No.2), 1
- Jansen, R.A., Windhorst, R., Alpaslan, M., et al. 2017a, *AAS* 229, 438.04
- Jansen, R.A., and the Webb Medium Deep Fields IDS GTO Team, the NEPTDS-VLA/VLBA Team, and the NEPTDS-Chandra Team 2017b, *AAS* 230, 216.02
- Jansen, R.A., Windhorst, R.A., Grogin, N.A., et al. 2018a, *AAS* 231, 354.14
- Jarrett, T.H., Masci, F., Tsai, C.W., et al. 2013, *AJ* 145, 6
- Joye, W.A., & Mandel, E. 2003, in: 'Astronomical Data Analysis Software and Systems XII', eds. H.E. Payne, R.I. Jedrezejewski, & R.N. Hook, *ASP Conf. Ser.* 295, 489
- Kaiser, N., Aussel, H., Burke, B.E., et al. 2002, *Proc. SPIE* 4836, 154
- Kalirai, J.S. 2018, *Contemp. Phys.*, 59, 251
- Kelsall, T., Weiland, J.L., Franz, B.A., et al. 1998, *ApJ* 508, 44
- Koekemoer, A.M., Faber, S.M., Ferguson, H.C., et al. 2011, *ApJS* 197, 36
- Kovalev, Y.Y., Petrov, L., Fomalont, E.B., & Gordon, D. 2007, *AJ* 133, 1236
- Krick, J.E., Surace, J.A., Thompson, D., et al. 2009, *ApJS* 185, 85
- Kurtz, M.J., Eichhorn, G., Accomazzi, A., Grant, C.S., & Murray, S.S. 2000, *A&AS* 143, 41
- Laity, A.C., Anagnostou, N., Berriman, B., et al. 2005, in: 'Astronomical Data Analysis Software and Systems XIV', eds. P. Shopbell, M. Britton, & R. Ebert, *ASP Conf. Ser.* 347, 34
- Lang, D. 2014, *AJ* 147, 108
- Larson, R.L., Finkelstein, S.L., Pirzkal, N., et al. 2018, *ApJ* 858, 94
- Laureijs, R.J., Duvet, L., Escudero Sanz, I., et al. 2010, *Proc. SPIE* 7731, 1H
- Leisenring, J.M., Rieke, M., Misselt, K., & Robberto, M. 2016, *Proc. SPIE* 9915, 2N
- Lightsey, P.A., Wei, Z., Skelton, D.L., et al. 2014, *Proc. SPIE* 9143, 3P
- Lightsey, P.A. 2016, *Proc. SPIE* 9904, 0A
- LSST Science Collaboration, Marshall, P., Anguita, T., et al. 2017, arXiv:1708.04058
- Luu, J.X., & Jewitt, D. 1998, *ApJ* 502, L91
- MacLeod, C.L., Brooks, K., Ivezić, Ž., et al. 2011, *ApJ* 728, 26
- Mainzer, A., Bauer, J., Grav, T., et al. 2011, *ApJ* 731, 53
- Mesinger, A., Johnson, B.D., & Haiman, Z. 2006, *ApJ* 637, 80
- Momcheva, I.G., Brammer, G.B., van Dokkum, P.G., et al. 2016, *ApJS* 225, 27
- Nicholl, M., Smartt, S.J., Jerkstrand, A., et al. 2013, *Nature* 502, 346
- Ofek, E.O., & Frail, D.A. 2011, *ApJ* 737, 45
- Oort, J.H. 1950, *BAN* 11, 91
- Oort, M.J.A., & Windhorst, R.A. 1985, *A&A* 145, 405
- Pan, T., Kasen, D., & Loeb, A., 2012, *MNRAS* 422, 2701
- Pasquali, A., Ferreras, I., Panagia, N., et al. 2006, *ApJ* 636, 115
- Petit, J.-M., Kavelaars, J.J., Gladman, B.J., et al. 2017, *AJ*, 153, 236
- Pirzkal, N., Xu, C., Malhotra, S., et al. 2004, *ApJS* 154, 501
- Pirzkal, N., Rothberg, B., Ly, C., et al. 2013, *ApJ* 772, 48
- Pirzkal, N., Malhotra, S., Ryan, R.E., et al. 2017, *ApJ* 846, 84
- Pontoppidan, K.M., Pickering, T.M., Laidler, V.G., et al. 2016, *Proc. SPIE* 9910, 16
- Radigan, J., Lafrenière, D., Jayawardhana, R., & Artigau, É. 2014, *ApJ* 793, 75
- Rajan, A., Patience, J., Wilson, P.A., et al. 2015, *MNRAS* 448, 3375
- Rieke, M.J., Kelly, D.M., & Horner, S.D. 2005, *Proc. SPIE* 590401
- Rodney, S.A., Riess, A.G., Strolger, L.-G., et al. 2014, *AJ* 148, 13
- Rodney, S.A., Riess, A.G., Scolnic, D.M., et al. 2015b, *AJ* 150, 156
- Ryan, R.E., Jr., Thorman, P.A., Yan, H., et al. 2011, *ApJ* 739, 83
- Ryan, R.E., Jr., & Reid, I.N. 2016, *AJ* 151, 92
- Ryan, R.E., Jr., Casertano, S., & Pirzkal, N. 2018, *PASP* 130, 034501
- Sarajedini, V.L., Koo, D.C., Klesman, A.J., et al. 2011, *ApJ* 731, 97
- Schlafly, E.F., & Finkbeiner, D.P. 2011, *ApJ* 737, 103
- Schlegel, D., Finkbeiner, D., & Davis, M. 1998, *ApJ* 500, 525
- Schmidt, K.B., Treu, T., Brammer, G.B., et al. 2014, *ApJ* 782, L36
- Schwamb, M.E., Brown, M.E., Rabinowitz, D.L., & Ragozzine, D. 2010, *ApJ*, 720, 1691
- Shankman, C., Kavelaars, J.J., Gladman, B.J., et al. 2016, *AJ*, 151, 31
- Skutskie, M.F., Cutri, R.M., Stiening, R., et al. 2006, *AJ* 131, 1163
- Straughn, A.N., Meurer, G.R., Pirzkal, N., et al. 2008, *AJ* 135, 1624
- Straughn, A.N., Pirzkal, N., Meurer, G.R., et al. 2009, *AJ* 138, 1022
- Strolger, L.-G., Dahlen, T., Rodney, S.A., et al. 2015, *ApJ* 813, 93
- Tody, D. 1986, *Proc. SPIE* 627, 733
- Tody, D. 1993, in "Astronomical Data Analysis Software and Systems II", eds. R.J. Hanisch, R.J.V. Brissenden, & J. Barnes, *ASP Conf. Ser.* 52, 173
- Treu, T., Schmidt, K.B., Brammer, G.B., et al. 2015, *ApJ* 812, 114
- Trujillo, C.A., Brown, M.E., Rabinowitz, D.L., & Geballe, T.R. 2005, *ApJ* 627, 1057
- Tyson, J.A. 2002, *Proc. SPIE* 4836, 10
- Vernstrom, T., Scott, D., Wall, J.V., et al. 2014, *MNRAS* 440, 2791

- Werner, M.W., Roellig, T.L., Low, F.J., et al. 2004, ApJS 154, 1  
Whalen, D.J., Even, W., Lovekin, C.C., et al. 2013, ApJ 768, 195  
Whalen, D.J., Smidt, J., Heger, A., et al. 2014, ApJ 797, 9  
Windhorst, R.A., Miley, G.K., Owen, F.N., Kron, R.G., & Koo, D.C. 1985, ApJ 289, 494  
Windhorst, R.A., Fomalont, E.B., Partridge, R.B., & Lowenthal, J.D. 1993, ApJ 405, 498  
Windhorst, R.A., Cohen, S.H., Hathi, N.P., et al. 2011, ApJS 193, 27  
Windhorst, R.A., Timmes, F.X., Wyithe, J.S.B., et al. 2018, ApJS 234, 41  
Wright, E.L., Eisenhardt, P.R.M., Mainzer, A.K., et al. 2010, AJ 140, 1868  
Yan, H., Ma, Z., Beacom, J.F., & Runge, J. 2018, ApJ (in press; arXiv:1808.01780)  
York, D.G., Adelman, J., Anderson, J.E. Jr., et al. 2000, AJ 120, 1579